Appendix A: Supporting information

1. Numerical model basic setup

The evolution of the South China Sea rift and passive margin system has been modelled using a two-dimensional version of the thermo-mechanical forward modelling software SLIM3D (Popov and Sobolev, 2008) (*Semi-Lagrangian Implicit Model for 3 Dimensions*). This finite-element code has been successfully applied in a number of geodynamic modelling studies at divergent (Brune and Autin, 2013; Brune et al., 2012; Brune et al., 2013; Heine and Brune, 2014), convergent (Quinteros and Sobolev, 2012a; Quinteros and Sobolev, 2012b; Quinteros et al., 2010) and transform (Popov et al., 2012) plate boundaries. SLIM3D solves the thermo-mechanically coupled conservation equations of momentum, energy, and mass. The code features a free surface at the top boundary, while at the bottom boundary isostatic equilibrium is realized by means of the Winkler foundation, where in- and outflow of material is accounted for during re-meshing (Popov and Sobolev, 2008).

Lithospheric deformation is implemented in terms of an elasto-visco-plastic rheology that is incorporated by decomposing the deviatoric strain rate into elastic, viscous, and plastic components. This method self-consistently reproduces diverse lithospheric-scale deformation processes like faulting, flexure and lower crustal flow. Viscous flow occurs via two creep mechanisms: diffusion and dislocation creep. The Mohr-Coulomb failure model is implemented for brittle deformation. The model involves four weakening mechanisms: shear heating, dislocation creep-related strain rate softening, friction softening, and viscous strain softening. Individual thermo-mechanical parameters are listed in Table S1.

Solving the energy equation, the model's temperature field results from the material-specific heat conductivity, radiogenic heat production, dissipation of mechanical energy and the following boundary conditions: The surface temperature is held constant at 0°C (or is proportional to sedimentary cover thickness where applicable), the bottom temperature is set to 1300°C and the lateral boundaries are thermally isolated.

Parameter	**Felsic Crust**	**Mafic Crust**	**Strong Mantle**	**Weak Mantle**
Density, (kg m^{-3})	2700	2850	3280	3300
Thermal expansivity, (10^{-5} K^{-1})	2.7	2.7	3.0	3.0
Bulk modulus, K (GPa)	55	63	122	122
Shear modulus, G (GPa)	36	40	74	74
Heat capacity, C_p (J kg^{-1} K^{-1})	1200	1200	1200	1200
Heat conductivity, λ (W K^{-1} m^{-1})	2.5	2.5	3.3	3.3
Radiogenic heat production, A (μW m^{-3})	1.5	1.5	0	0
Initial friction coefficient, μ (-)*	0.5	0.5	0.5	0.5
Cohesion, c (MPa)	5.0	5.0	5.0	5.0
Pre-exponential constant for diffusion creep, log(B_{Diff}) (Pa^{-1} s^{-1})	-	-	-8.65	-8.66
Activation energy for diffusion creep, E_{Diff} (kJ / mol)	-	-	375	335
Activation volume for diffusion creep, V_{diff} (cm^{-3} / mol)	-	-	6	4
Pre-exponential constant for dislocation creep, log(B_{Disloc}) (Pa^{-n} s^{-1})**	-17.3	-15.40	-15.56	-15.05
Power law exponent for dislocation creep, n	2.3	3.0	3.5	3.5
Activation energy for dislocation creep, E_{Disloc} (kJ / mol)	154	356	530	480
Activation volume for dislocation creep, V_{Disloc} (cm^{-3}/mol)	0	0	13	10

Table S1. Thermo-mechanical parameters. *During frictional strain softening, the friction coefficient μ reduces linearly from 0.5 to 0.05 for brittle strain between 0 and 1. For strains larger than 1, it remains constant at 0.05. **Similary, during viscous strain softening, B_{Disloc} is multiplied by a factor that grows linearly from 1 to 100 for viscous strain between 0 and 1. Maximum viscous weakening with a factor of 100 leads to a viscosity reduction of $100^{-1/n}$, whereas the stress exponent n ranges between 2.3 (crust (Ranalli and Murphy, 1987)) and 3.5 (mantle (Brune et al., 2014)). Hence the maximum reduction in viscosity because of this softening mechanism will be 7.4 for crust and 3.7 for mantle material.

2. Setup of simple model without extension

In order to evaluate the influence of lower crustal viscosity on crustal flow during sediment loading, we run a laterally homogeneous model without any extension. The model involves a 10 km thick upper crustal layer that deforms via wet quartzite flow law (Ranalli and Murphy, 1987) and an 80 km thick mantle layer of dry olivine (Hirth and Kohlstedt, 1996). Moreover, we use an isoviscous lower crust of 10 km thickness (Fig. S1) whose viscosity is

varied between 10^{18} and 10^{21} Pa.s . The overall crustal thickness of 20 km and the depth of the thermal lithosphere-asthenosphere boundary of 60 km are similar to the main model at the time of strong sedimentation (Fig. 5 of the main article). Because no upwelling mantle flow takes place in the simplified model, the asthenospheric mantle is neglected. This simple model involves a computational domain of 100 km depth and 600 km width. Using a resolution of 1 km, the model consists of 60,000 elements and 121,402 nodes.

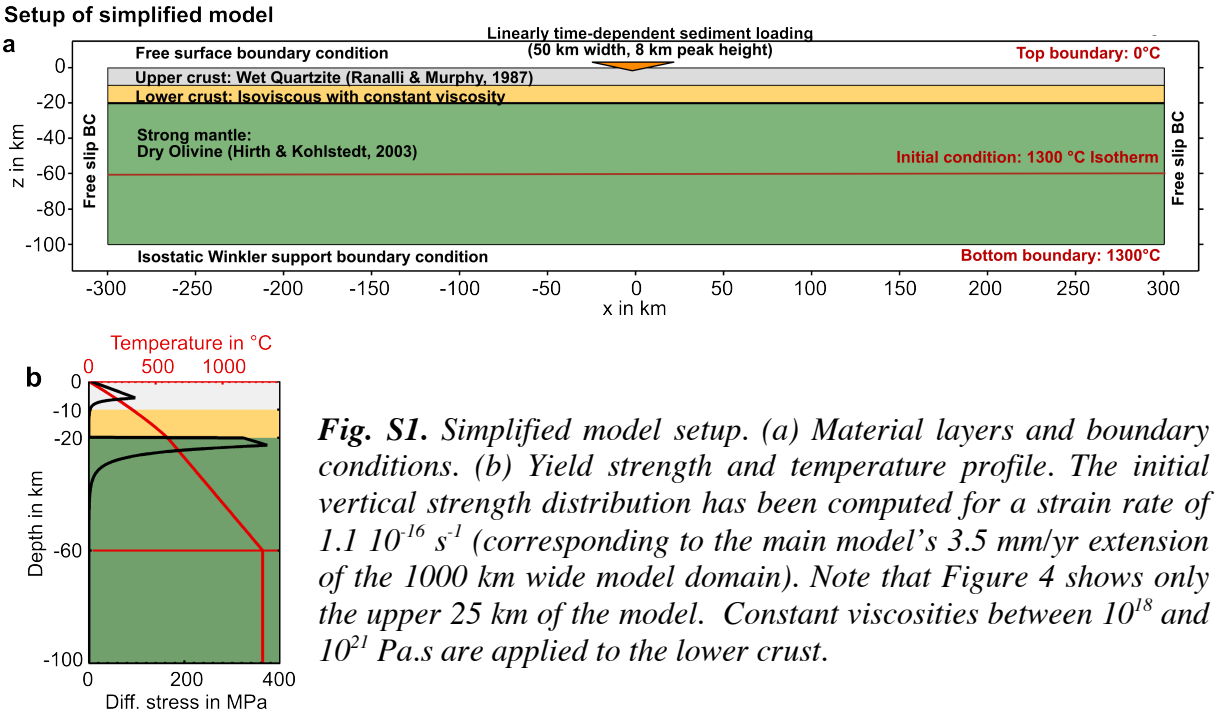

Fig. S1. *Simplified model setup. (a) Material layers and boundary conditions. (b) Yield strength and temperature profile. The initial vertical strength distribution has been computed for a strain rate of 1.1 10^{-16} s^{-1} (corresponding to the main model's 3.5 mm/yr extension of the 1000 km wide model domain). Note that Figure 4 shows only the upper 25 km of the model. Constant viscosities between 10^{18} and 10^{21} Pa.s are applied to the lower crust.*

3. Setup of the main numerical model

In order to reproduce the general characteristics of the South China Sea Evolution, we extend the previous model by accounting for temperature- and stress-dependent viscosity in all layers, introducing extensional velocities at the lateral boundaries, and by adopting the following initial configuration: We use four distinct petrological layers: felsic crust, mafic crust, strong mantle and weak mantle. The upper 25 km of our model consists of felsic crust that deforms in accordance with a weak wet quartzite flow law (Ranalli and Murphy, 1987), representing the weak crust of pre-rift South China which was a continental magmatic arc during the Mesozoic (Gilder et al., 1996). The weakness of the crust has strong impact on rift style and final margin symmetry: Only very weak crust generates wide and symmetric margins like those of the South China Sea (Brune et al., 2014; Huismans and Beaumont,

2011). The initial crustal thickness of 33 km is supported by seismically inferred crustal thickness within the South China block (Nissen et al., 1995). A mafic lower crustal layer of 8 km thickness deforms via a wet anorthite flow law (Rybacki and Dresen, 2000). We use dry olivine rheology (Hirth and Kolhstedt, 2003) to model deformation of the strong, depleted, subcontinental mantle extending to 90 km depth, while we use a wet olivine (i.e., 500 ppm H/Si) flow law (Hirth and Kolhstedt, 2003) for the weak, asthenospheric mantle covering the lowermost 30 km of the model domain. Our model consists of a rectangular segment of 122 km depth and 1000 km width. With a resolution of 1 km, it involves 122,000 elements and 246,246 nodes. As an initial condition, a small thermal heterogeneity is introduced in the model centre in order to avoid rift localisation at the model boundaries. This heterogeneity is generated by elevating the 1300°C isotherm in form of a triangular shape with 20 km height and 20 km width (Fig. S2). The thermal steady-state is computed before model start and was used as the initial condition to run the model.

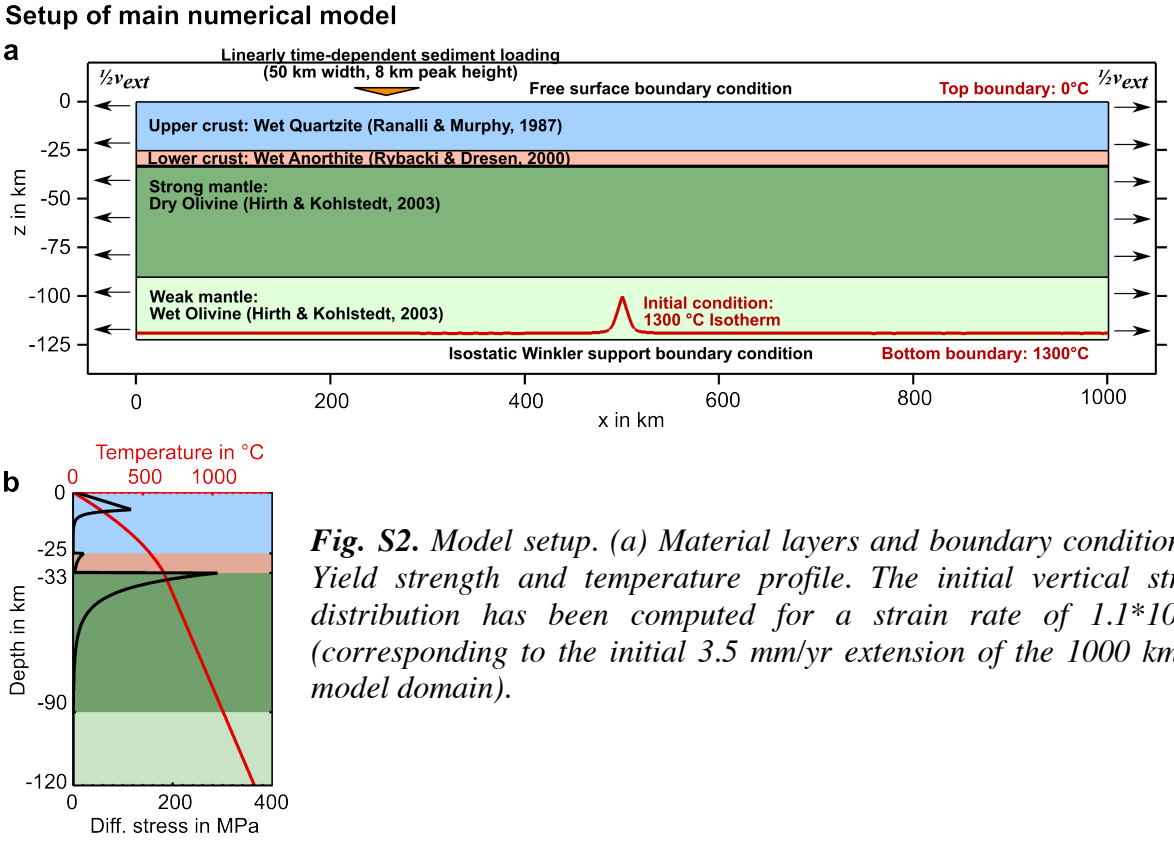

Fig. S2. *Model setup. (a) Material layers and boundary conditions. (b) Yield strength and temperature profile. The initial vertical strength distribution has been computed for a strain rate of* $1.1*10^{-16}$ s^{-1} *(corresponding to the initial 3.5 mm/yr extension of the 1000 km wide model domain).*

4. Sedimentation

The numerical code features a free surface boundary condition at the top of the model allowing for dynamic evolution of topography. In this study, the surface boundary condition has been complemented by a routine that accounts for sediment deposition. This has been done in very simple and transparent way that nevertheless captures the key aspect of this study: Instead of introducing sediments as a proper material phase, we prescribe a local boundary force that corresponds to an arbitrary sediment distribution. Although this approach does not allow to resolve the internal structure of the sediments, it robustly incorporates the effect of a space- and time-dependent sediment load on the crystalline basement. We approximate the sedimentation distribution of the deep Baiyun Sag basin that we aim to understand here through a simple triangular shape of 50 km width and 8 km height, which results in a maximum load of 200 MPa, assuming a sediment density of 2500 kg/m^3. In agreement with geophysical interpretation (see main part), time-dependent sedimentation is approximated through a linear increase in sediment load starting at 22 Ma and reaching peak sediment thickness of 8 km at 12 Ma. In all figures, sediment distribution is depicted by the orange triangle.

Sedimentation influences the underlying crust not only through its mechanical load but also in terms of thermal insulation. We account for this affect by correlating surface temperature with sediment thickness through a constant thermal gradient of 30°C/km. This procedure yields a final peak temperature of 250°C at the bottom of the basin.

References

Brune, S., Autin, J., 2013. The rift to break-up evolution of the Gulf of Aden: Insights from 3D numerical lithospheric-scale modelling. Tectonophysics, 607: 65–79.

Brune, S., Heine, C., Perez-Gussinye, M., Sobolev, S.V., 2014. Rift migration explains continental margin asymmetry and crustal hyper-extension. Nature Communications, in press.

Brune, S., Popov, A.A., Sobolev, S.V., 2012. Modeling suggests that oblique extension facilitates rifting and continental break-up. Journal of Geophysical Research, 117(B08402).

Brune, S., Popov, A.A., Sobolev, S.V., 2013. Quantifying the thermo-mechanical impact of plume arrival on continental break-up. Tectonophysics, 604: 51–59.

Gilder, S.A., Gill, J.B., Coe, R.S., Zhao, X., Liu, Z., Wang, G., Yuan, K., Liu, W., Kuang, G., Wu, H., 1996. Isotopic and paleomagnetic constraints on the Mesozoic tectonic evolution of South China. Journal of Geophysical Research, 101: 16,137–16,155.

Heine, C., Brune, S., 2014. Oblique rifting of the Equatorial Atlantic: Why there is no Saharan Atlantic Ocean. Geology, G35082.1.

Hirth, G., Kohlstedt, D.L., 1996. Water in the oceanic upper mantle; implications for rheology, melt extraction and the evolution of the lithosphere. Earth and Planetary Science Letters, 144(1-2): 93-108.

Hirth, G., Kolhstedt, D.L., 2003. Rheology of the upper mantle and the mantle wedge: A view from the experimentalists. In: Eiler, J. (Ed.), Inside the Subduction Factory. American Geophysical Union, Washington, DC, pp. 83–105.

Huismans, R., Beaumont, C., 2011. Depth-dependent extension, two-stage breakup and cratonic underplating at rifted margins. Nature, 473: 74-79.

Nissen, S.S., Hayes, D.E., Buhl, P., Diebold, J., Yao, B., Zeng, W., Chen, Y., 1995. Deep penetration seismic soundings across the northern margin of the South China Sea. Journal of Geophysical Research, 100(B11): 22,407-22,433.

Popov, A.A., Sobolev, S.V., 2008. SLIM3D: A tool for three-dimensional thermo mechanical modeling of lithospheric deformation with elasto-visco-plastic rheology. Physics of the Earth and Planetary Interiors, 171: 55–75.

Popov, A.A., Sobolev, S.V., Zoback, M.D., 2012. Modeling evolution of the San Andreas Fault system in northern and central California. Geochemistry Geophysics Geosystems, 13(Q08016).

Quinteros, J., Sobolev, S.V., 2012a. Constraining kinetics of metastable olivine in the Marianas slab from seismic observations and dynamic models. Tectonophysics, 526–529: 48–55.

Quinteros, J., Sobolev, S.V., 2012b. Why has the Nazca plate slowed since the Neogene? Geology, 41: 31–34.

Quinteros, J., Sobolev, S.V., Popov, A.A., 2010. Viscosity in transition zone and lower mantle: Implications for slab penetration. Geophysical Research Letters, 37(L09307).

Ranalli, G., Murphy, D.C., 1987. Rheological stratification of the lithosphere. Tectonophysics, 132: 281–295.

Rybacki, E., Dresen, G., 2000. Dislocation and diffusion creep of synthetic anorthite aggregates. Journal of Geophysical Research, 105: 26,017–26,036.